Optics Communications 435 (2019) 271–276

Contents lists available at ScienceDirect

Optics Communications

journal homepage: www.elsevier.com/locate/optcom

Concurrent monitoring of zeroth-order and diffraction-order interference fringes for mosaicking echelle

Min Cong [a,b], Xiangdong Qi [a,*], Xiaotao Mi [a,b], Xiaotian Li [a], Haili Yu [a], Shanwen Zhang [a], Hongzhu Yu [a], Bayanheshig [a]

[a] Grating Technology Laboratory, Changchun Institute of Optics and Fine Mechanics and Physics, Chinese Academy of Sciences, Changchun, Jilin 130033, China
[b] University of Chinese Academy of Sciences, Beijing 100049, China

ARTICLE INFO

Keywords:
Mosaicked echelle
Interferometry
Diffraction

ABSTRACT

A mosaicking method for echelles is proposed. The "zero-order" and diffraction-order interference fringes of the echelle can be imaged simultaneously on the detector using a mirror–echelle structure designed. The five-dimensional mosaicking errors are divided into two categories for elimination using the "zero order" and the diffraction order. During the experiments, adjustment devices for the mosaicking errors are installed on two echelles for these two categories to avoid mechanical coupling. As theoretical analysis, we follow the experimental steps to obtain a mosaicked echelle.

1. Introduction

In the 1990s, optical telescopes with diameters of up to 10 m were built worldwide. High-resolution spectrometers were widely required for these telescopes, but the apertures of the available gratings [1] could not meet the requirements of astronomy applications. The mosaicked echelle was then proposed [2] and most large telescopes were equipped with a mosaicked echelle to increase their spectral resolution for astronomical observation [3]. More recent, telescopes such as the Hobby–Eberly telescope [4], the James Webb Space Telescope [5] and the Thirty Meter Telescope (TMT) [6] will require large-sized mosaicked echelles. In addition, the OMEGA EP system [7–9], Pric2000 [10,11] and FIREX-1 [12] demonstrate the importance of large-sized mosaicked gratings for inertial confinement fusion (ICF) applications.

There are three main methods for mosaicking of gratings: far-field patterning [13–16], interferometry [17–20] and object–image–grating self-tiling [21]. In the far-field patterning method, the shapes of the zero-order and diffraction-order far-field diffraction spots of the two mosaicked gratings are monitored, when both of the zero-order and diffraction-order spots of the two gratings are overlap as one ideal airy disk, the mosaicking errors meet the requirements of the specific application. The OMEGA EP laser system [7,8] and Zeng et al. [13–15] adopted this method for mosaicking gratings based on specified Strehl ratio and R80 targets. And Zeng et al. propose a double-wavelength method to achieve a better mosaicked grating. The object–image–grating self-tiling method can eliminate the mosaicking errors by using the relationship between the object and the image along with the far-field spot. However, when the diffraction spots of the two gratings overlap, the residual mosaicking errors remain large, which can be seen by the interference map. Then the interferometry method is proposed, which is based on interferometry and uses the wavefronts of the mosaicked gratings as the main targets [9]. The shapes of the far-field diffraction spots of the two mosaicked gratings are well adjusted and the interference fringes produced by the two gratings are then observed. After the zero-order and diffraction-order interference fringes of the two gratings are both moved to the same, the mosaicked grating is completed. And Lu et al. [19] propose a double-angle incident light method to eliminate the mosaicking errors completely. However, the interferometry method mentioned above is not suitable for mosaicked echelle, the detector cannot detect the zero order because of the extremely low zero-order efficiency.

Based on the characteristics of the echelle, an interference method that is suitable for mosaicking echelles is proposed in this work. To avoid low zero-order efficiency, we design a new structure called the mirror–echelle structure to image simultaneously the zero-order and diffraction-order interference fringes on the screen to remove the five-dimensional mosaicking errors. A theoretical model of echelle mosaicking is established, and the steps of the mosaicking experiment are summarized. The experiment is carried on with two echelles, the peak-to-valley (PV) values are 0.494λ and 0.452λ, where λ is the operating wavelength. The adjustment mechanisms for the mosaicking errors are installed

* Correspondence to: No.3888 Dong Nanhu Road, Changchun, Jilin 130033, China.
E-mail address: chinagrating@263.net (X. Qi).

https://doi.org/10.1016/j.optcom.2018.11.030
Received 26 September 2018; Received in revised form 6 November 2018; Accepted 11 November 2018
Available online 26 November 2018

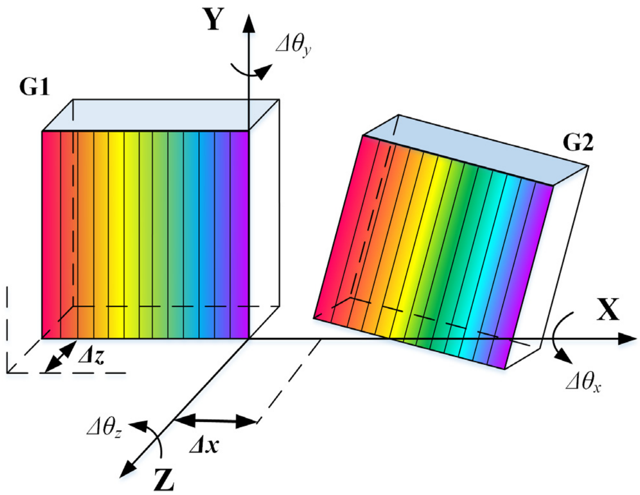

Fig. 1. Five degrees of freedom between two adjacent echelles.

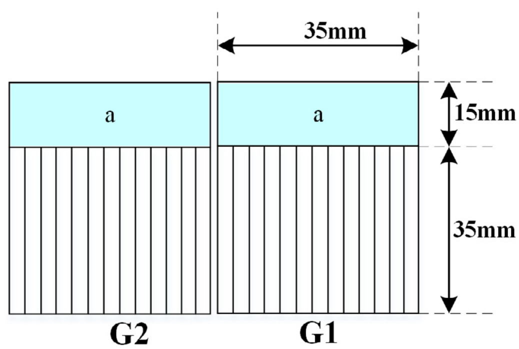

Fig. 2. The mirror-ecehlle structure.

on two echelles to avoid mechanical coupling. Then, a mosaicked echelle is obtained, the PV value is 0.592λ, the diffraction energy is largely concentrated within the central Airy disk, and the Strehl ratio is 0.947.

2. Theoretical analysis of the mosaicking echelle

As shown in Fig. 1, within the coordinate set up, G1 is the reference grating, while G2 is the moving grating. The x-axis is along the indexing direction, the y-axis is along the groove direction, the z-axis is perpendicular to the grating surface.

There are five-dimensional mosaicking errors. The tip angle is the rotation around the x-axis, and is represented by $\Delta\theta_x$; the tilt angle is the rotation around the y-axis, and is represented by $\Delta\theta_y$; the in-plane angle is the rotation angle around the z-axis and is represented by $\Delta\theta_z$; the grating space is the distance between the two gratings along the x-axis, represented by Δx; and the longitudinal offset is the distance between the two gratings along the z-axis, and is represented Δz. The characteristics of the mosaicking errors mean that they can be divided into in-plane errors ($\Delta\theta_z$ and Δx) and coplanar errors ($\Delta\theta_x$; $\Delta\theta_y$ and Δz), and they can be eliminated by using the diffraction order and the zero order, respectively.

By comparing the mosaicking errors with the theory of the diffraction wavefront [22,23], the optical path difference (OPD) between the two gratings can be obtained as shown in Eq. (1):

$$\Delta = n_1 \cdot (-y_i\Delta\theta_x + x_i\Delta\theta_y + \Delta z)(\cos\theta_i + \cos\theta_k) + n_2 \cdot (y_i\Delta\theta_z + \Delta x)\frac{m\lambda}{d}, \quad (1)$$

where θ_i is the angle of incident light, θ_k is the angle of diffracted light, m is the diffraction order, d is the grating constant, and (y_i, x_i) is the position on the grating surface, n_1 and n_2 are the integers, and Δ is OPD. The first component of the equation describes the coplanar errors, while the second item describes the in-plane errors.

The OPD can be shown as an interference fringe pattern by using an interferometer, as described by Eq. (2).

$$I = A \cdot \left[1 + \cos(\frac{2\pi}{\lambda} \cdot \Delta)\right], \quad (2)$$

where A is the light intensity constant, and I is the light intensity. The theoretical model of the mosaicked grating indicates that the effects of the five dimensional mosaicking errors on the interference fringes produced by light diffraction differ, $\Delta\theta_z$ and $\Delta\theta_x$ can make the interference fringes have different periods, and $\Delta\theta_y$ can make the interference fringes have different slopes, and Δx and Δz can make the interference fringes misalignment.

Because the zero-order reflected light of the echelle is very weak, a new type of mirror–echelle structure is designed in which the aluminum film is reserved as a mirror during the echelle ruling process to replace the zero order. The size of the mirror–echelle structure are as shown in Fig. 2, two mirror–echelle structures are placed side-by-side. The blue part represents the reserved aluminum film that acts as the mirror rather than the zero order to eliminate the coplanar errors.

When this special echelle structure is used, the zero-order and the diffraction-order interference fringes can be imaged on the detector simultaneously, the five mosaicking errors can be demonstrate on the interference fringes respectively, in particular, Δz can be eliminated by combining the mirror–echelle structure with the double-angle incident light. The optical path is illustrated in Fig. 3, where θ_{i1} is the angle of the incident light, and θ_{i2} is the angle of the double-angle incident light.

The black line is the diffraction order in the Littrow structure. The red solid line represents the zero order of the mosaicking echelle represented

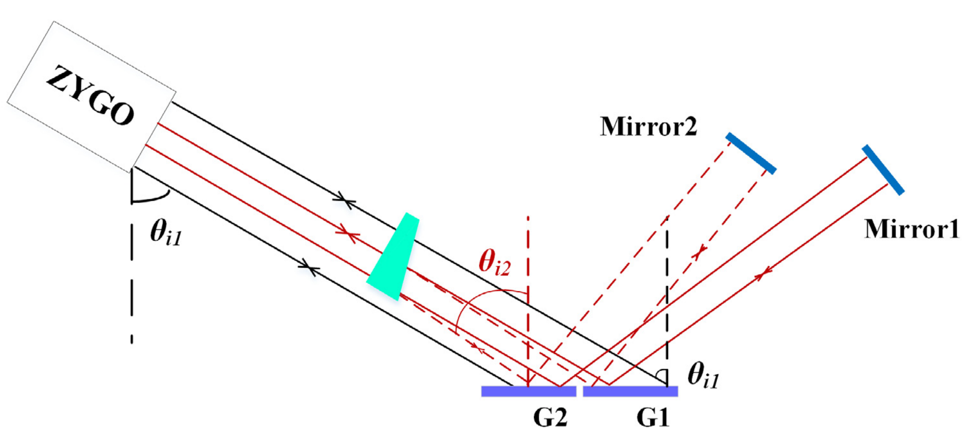

Fig. 3. The optical path.

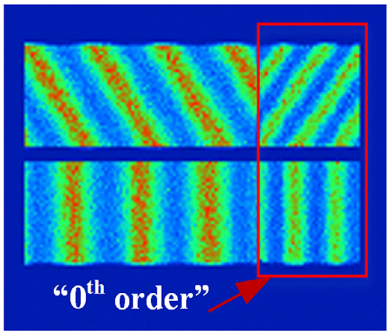

Fig. 4. "Zero-order" and diffraction-order interference fringes.

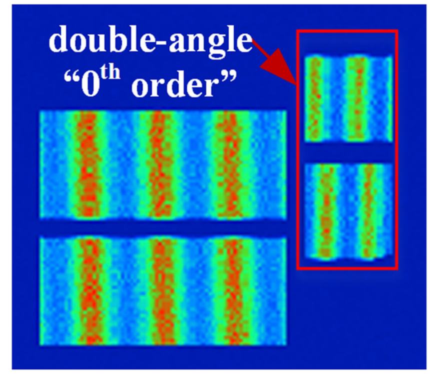

Fig. 5. Double-angle "zero-order" and diffraction-order interference fringes.

by the aluminum film mirror on the echelle plane, and it can return to the interferometer by using Mirror1. The red broken line represents the double-angle incident light generated by the prism, it can return to the interferometer by using Mirror2, it is used to remove Δz. When the Mirror1 is used, the interference fringes of the mosaicking echelle are as shown in Fig. 4.

In Fig. 4, the upper portion is one of the echelles and the lower portion is the other echelle. The interference fringes in the red box are the "0th order" and the left side is the diffraction order.

The interference fringes that are generated by the "0th order" on the right side show the influence of the coplanar errors, the OPD is shown as Eq. (3).

$$\Delta_{01} = 4 \cdot \cos\theta_{i1} \cdot (-y_i \cdot \Delta\theta_x + x_i \cdot \Delta\theta_y + \Delta z), \tag{3}$$

The stripes that are generated by the diffraction order on the left side show the effects of all the mosaicking errors, and the OPD is shown as Eq. (4).

$$\Delta_m = 2\cos\theta_{i1}(-y_i\Delta\theta_x + x_i\Delta\theta_y + \Delta z) + (y_i\Delta\theta_z + \Delta x)\frac{m\lambda}{d}. \tag{4}$$

When the coplanar angle errors are removed using the "0th order" to make the interference fringes of the two echelles have the same period and the same inclination, the in-plane angle error should be adjusted to make the period of the diffraction-order interference fringes consistent, and the displacement errors are then in the schedule.

First, Δz is adjusted. One echelle is moved along the z-axis to align the "zero-order" interference fringes of the two echelles, and the resulting "zero-order" OPD is shown in Eq. (5).

$$\Delta_0 = 4 \cdot \Delta z \cdot \cos\theta_{i1} = k_1 \cdot \lambda. \tag{5}$$

where k_1 is an integer in the same manner as k_2, k_3 and k, which will appear below.

Second, Δx is adjusted. The other echelle is then moved along the x-axis to align the diffraction-order interference fringes, and the resulting diffraction-order OPD is shown in Eq. (6).

$$\Delta_m = 2 \cdot \Delta z \cdot \cos\theta_{i1} + \Delta x \cdot \frac{m\lambda}{d} = k_2 \cdot \lambda. \tag{6}$$

Finally, Mirror1 is taken away and a prism is added to the optical path to generate the double-angle incident light, as indicated by the red broken line in Fig. 3. At this moment, the interference fringes are as shown in Fig. 5.

The interference fringes on the left side are the diffraction-order fringes, and the right side in the red box shows the "0th order" formed by the double-angle incident light. The double angle allows Δz to be moved to zero when the two parts of the interference fringes in Fig. 5 are both aligned.

The OPD on the right side, which is the 0th order, is shown in Eq. (7).

$$\Delta_{02} = 4 \cdot \Delta z \cdot \cos\theta_{i2}. \tag{7}$$

There are now two cases of the OPD in Eq. (5) with regard to Δz of the "zero order".

$$k_1 = 2 \cdot k, \quad or \quad k_1 = 2 \cdot k + 1. \tag{8}$$

In both cases, the two-part interference fringes of the diffraction order can be aligned, corresponding to Δx, as shown in Eq. (9).

$$\Delta x = k_2 \cdot \frac{d}{m}, \quad or \quad \Delta x = k_2 \cdot \frac{d}{m} + \frac{1}{2} \cdot \frac{d}{m}. \tag{9}$$

If the above experiment represents the first case, then:

$$\begin{cases} k_1 = 2 \cdot k \\ \Delta x = k_2 \cdot \dfrac{d}{m}. \end{cases} \tag{10}$$

When the interference fringes of the "zero order" that were refracted by the prism and the diffraction order are both aligned, Δz is then either 0 mm or 0.3467 mm or larger. However, a gap of 0.3467 mm would be a visible gap, which can clearly be excluded. Therefore, this is the correct mosaicking situation.

If the above experiment represents the second case, then:

$$\begin{cases} k_1 = 2 \cdot k + 1 \\ \Delta x = k_2 \cdot \dfrac{d}{m} + \dfrac{1}{2} \cdot \dfrac{d}{m}. \end{cases} \tag{11}$$

When the interference fringes of the "zero order" refracted by the prism and those of the diffraction order are both aligned, Δx and Δz contribute an OPD of $k_3\lambda + \lambda/2$. The minimum values are that Δz is 31.4201 μm and Δx is 175.8087 nm in this case. If we continue to move the echelle along the z-axis by another 31.4201 μm, then the interference fringes of the zero order that were refracted by the prism and the diffraction order will be aligned again. Based on this phenomenon, we can correct this mistake. If one echelle is moved along the x-axis by a distance of 175.8087 nm, this situation can be converted into the correct mosaicking situation.

Therefore, the initial of Δz must be less than 0.3467 mm to allow completion of the mosaicking experiment.

3. Experimental results

A Zygo interferometer is used at a wavelength of 632.8 nm. The two echelles in the experiment have the same parameters, as following: the grating density is 79 gr/mm, the diffraction order is the −36th order, the blaze angle is −64.1373°. And the peak-to-valley (PV) values of the two gratings are 0.494 λ and 0.452 λ, where λ is the operating wavelength.

Based on the description above, the steps required for mosaicking of the echelles can be summarized as follows.

In preparation for the mosaicking experiment, the adjustment devices are installed on echelles of the two different types. The two far-field diffraction spots of the "0th order" are adjusted to overlap by moving the echelle using the coplanar-error adjustment devices; they

Table 1
The efficiency of 36th order, 0th order and the aluminum mirror of two mirror–echelle structures.

The efficiency of the zero order and the aluminum mirror		
Echelle	Area on the mirror–echelle	Absolute efficiency
Top1	Mirror	0.4232
	0th order	0.0954
	36th order	0.2686
Top2	Mirror	0.4095
	0th order	0.0913
	36th order	0.2600

are then positioned at the center of the screen by moving Mirror1, and the coplanar errors are thus coarsely removed. The two far-field diffraction spots of the −36th order are adjusted to overlap by moving the echelle using the in-plane-error adjustment devices; they are then positioned at the center of the screen by moving the Zygo interferometer, and the in-plane errors are thus coarsely removed. We then check the interference fringes of both the "0th order" and the −36th order. The Zygo interferometer is adjusted until the −36th-order interference fringes of the echelle with the in-plane-error adjustment devices are vertical. Mirror1 is then adjusted until the "0th-order" interference fringes of the echelle with the in-plane-error adjustment devices are vertical and the period is appropriate. The experiment begins and the mosaicked echelles will not be touched.

(1). Adjust the coplanar angle errors ($\Delta\theta_x$, $\Delta\theta_y$) using the "0th-order" interference fringes. The echelle with the in-plane-error adjustment devices acts as the reference grating. Then, $\Delta\theta_x$, and $\Delta\theta_y$ are tuned so that the 0th-order interference fringes of the two echelles have the same period and are oriented parallel to each other, and the coplanar angle errors are removed.

(2). Adjust the in-plane angle error ($\Delta\theta_z$) using the −36th-order interference fringes. The echelle with the coplanar-error adjustment devices acts as the reference echelle. The echelle with the in-plane-error adjustment devices must be moved until the diffraction-order interference fringes of two echelles have the same period and the in-plane angle errors are thus removed.

(3). Remove the longitudinal offset (Δz) and the grating space (Δx) using the "0th-order" interference fringes in cooperation with the −36th-order fringes. The "0th-order" interference fringes of the two echelles are aligned to eliminate Δz by moving the echelle using the coplanar-error adjustment devices. The −36th-order interference fringes are then aligned by moving the echelle using the in-plane-error adjustment devices to eliminate Δx.

(4). Remove the periodic effects of Δz using double-angle incident light. The prism is placed into the optical path. The "0th-order" interference fringes that are generated by the light refracted from the prism and the −36th-order interference fringes of the echelles are both aligned by moving the echelle using the coplanar-error adjustment devices.

(5). The correctness of the experiment must now be tested. The stroke of the adjustment mechanism for Δz is 250 μm. If there are multiple cases in which the −36th-order and 0th-order interference fringes are aligned simultaneously when the ecehlle is move along z-axis only, then it is the wrong case. The echelle with the in-plane-error adjustment devices should be moved by a distance of 175.8087 nm along the x-axis, and steps 3 and 4 are repeated to complete the experiment when Δz is removed.

By following the experimental steps described above, the mosaicking experiment should then be set up. The ecehlle efficiencies of the −36th order, the 0th order, −36th order and the aluminum mirror are shown in Table 1.

In Table 1, the efficiency of the 0th order of the echelle is 0.0954 and 0.0913, so the mirror–echelle structure is thus designed such that the aluminum film replaces the 0th order of the echelle.

The interference fringes and a three-dimensional map of the 0th order of the mirror–echelle structure are shown in Fig. 6, where the PV value of the 0th order on the mirror–echelle structure is 0.392λ, and the root-mean-square (rms) value is 0.036λ. In the three-dimensional map, the distance between the echelle surface and the aluminum surface is 0.07λ, and the aluminum film surface is smooth overall, with a PV value of 0.044λ. The two echelles are generated from the same replica of the same master echelle, so the other echelle has the same structure. Therefore, the reserved aluminum film can replace the 0th order of the echelle in the mosaicking experiment.

The experimental optical path is shown in Fig. 7, includes a prism, a mirror, the mosaicked echelle and the Zygo interferometer. The angle of the incident light is 64.1373°; the coplanar-error adjustment devices and in-plane-error adjustment devices are installed on the two echelles,

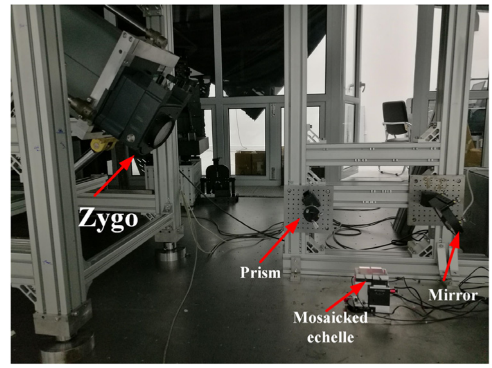

Fig. 7. Layout of the optical path.

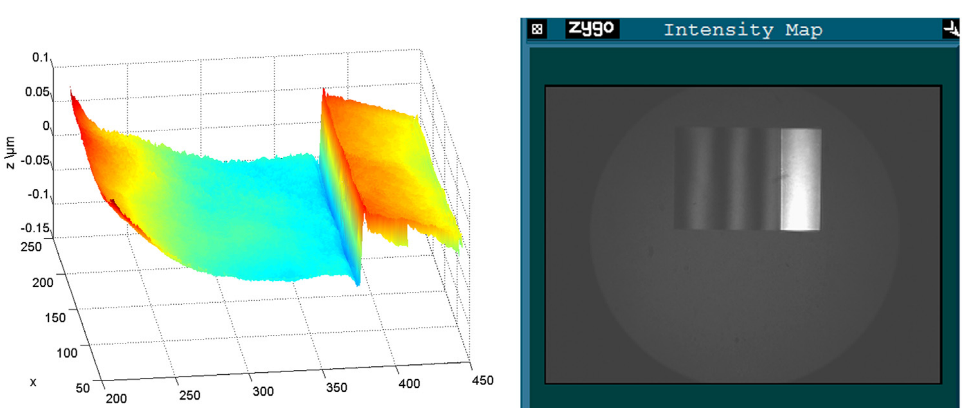

Fig. 6. The interference fringes and three-dimensional map on 0th order.

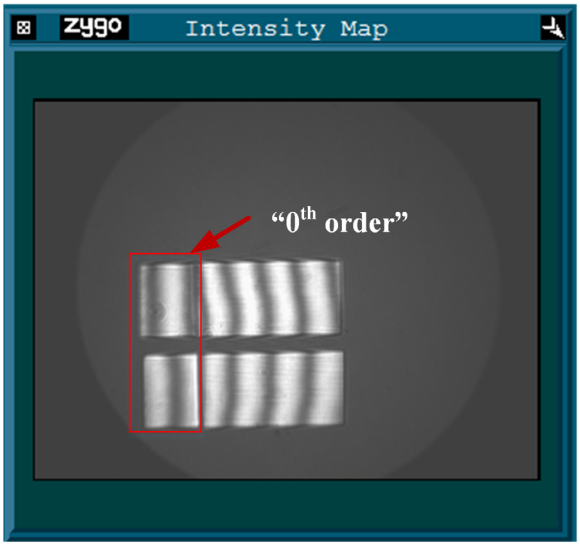

Fig. 8. Interferogram of "0th order" and −36th order.

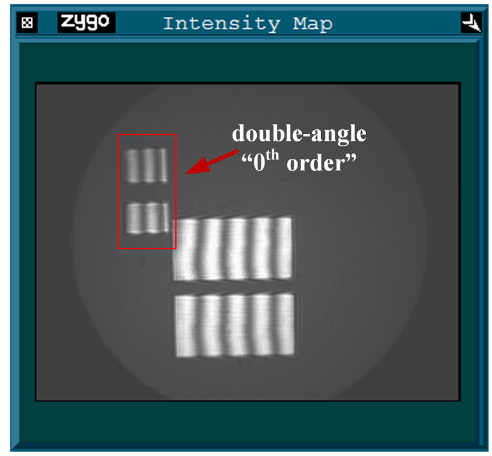

Fig. 9. Interferogram of double-angle "0th order" and 36th order.

and the mosaicked echelle lies flat on the ground. The prism and the mirror can both be moved anytime.

In the experiments, an interferogram is obtained from the Zygo interferometer as shown in Fig. 8. The red box on the left side contains the 0th order, which is reflected by Mirror1. The right side shows the −36th order of the echelle in the Littrow configuration.

In accordance with the experimental steps described above, the echelle with the coplanar-error adjustment devices is moved to eliminate both $\Delta\theta_x$ and $\Delta\theta_y$ by using the "0th-order" interference fringes on the left side. The echelle with the in-plane-error adjustment devices is then moved to eliminate $\Delta\theta_z$ by using the −36th-order interference fringes on the right side.

After the angle errors are removed, the angle adjustment devices should then be locked. The echelle with the coplanar-error adjustment devices is moved along the z-axis to remove Δz by aligning the "0th-order" interference fringes; the echelle with the in-plane-error adjustment devices is then moved along the x-axis to remove Δx by aligning the −36th-order interference fringes. However, Δz may bring $k\lambda$ to affect the OPD, so the prism must be added into the optical path.

In Fig. 9, the interference fringes of the 0th order, which are generated by the light refracted from the prism, are in the red box shown on the left side. The −36th-order fringes are shown on the right side. The echelle with the coplanar-error adjustment devices is moved along the z-axis until the interference fringes of the 0th order and the −36th order are aligned simultaneously. The correctness of the experiment must then be tested as described in experimental step 5, where steps 3 and 4 will be repeated until Δz is removed.

We then obtain a mosaicked echelle. The interference fringes of the two echelles have the same period, are parallel and are aligned with each other, as shown in Fig. 10.

The PV value of the mosaicked echelle is 0.592λ, and its rms value is 0.049λ, as shown in Fig. 11.

Checking of the three-dimensional map of the mosaicked echelle shows that the surfaces of the two echelles are basically in the same plane; the edges of the echelles contribute most of the PV value, which represents the quality of the echelles themselves, only (see Fig. 12).

As measured by the Zygo interferometer, a Strehl ratio of the mosaicked echelle is 0.947 in which the diffraction energy is largely concentrated in the central Airy disk, as shown in Fig. 13. (See Table 2).

During the mosaicking experiments, the postures of the echelles are adjusted via the mechanical structures to avoid artificial touching.

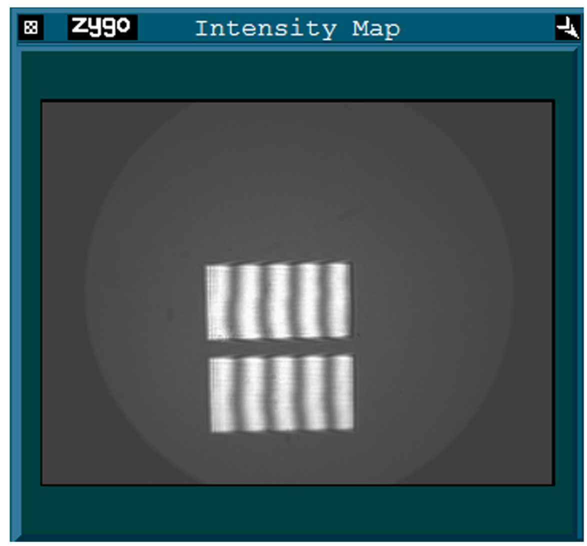

Fig. 10. Interferogram of the mosaicked echelle.

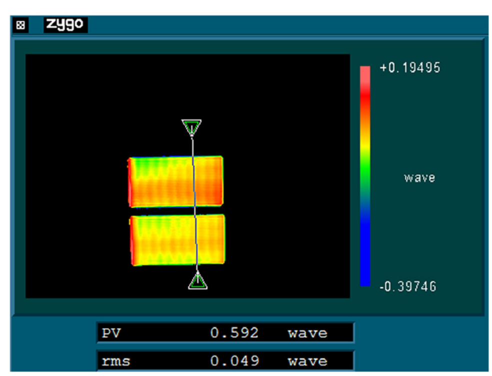

Fig. 11. PV value and the rms of the mosaicked echelle.

The interference fringes of the "0th order" and the −36th order were adjusted by turning the Zygo interferometer and the mirrors. In addition, the echelles were lying on the ground for greater stability.

While in the large-scale mosaicked ecehlle, the wavefront detection of the substrates will be performed and qualified to manufacture an echelle, the reserved aluminum film is good enough to be treated as

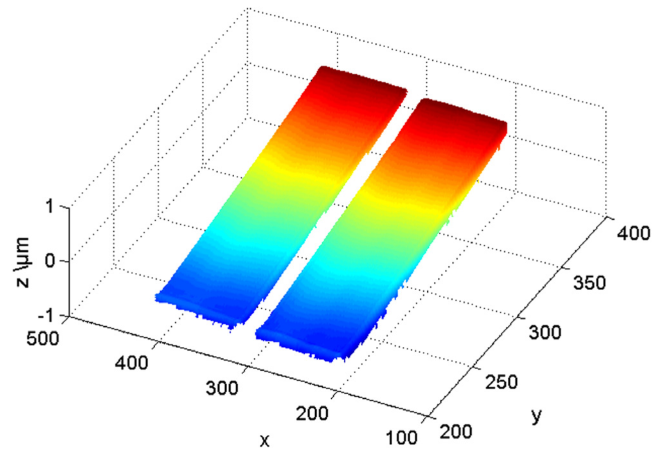

Fig. 12. Three-dimensional map of −36th order of the mosaicked echelle.

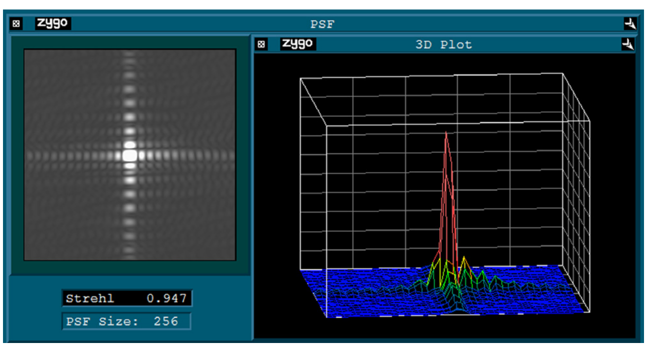

Fig. 13. Strehl ratio and diffraction spot of the mosaicked echelle.

Table 2
Results of the mosaicking experiments.

	Top1	Top2	Mosaicked ecehlle
PV(λ)	0.494	0.452	0.592
RMS(λ)	0.056	0.046	0.049
Streh1	–	–	0.947

the zero order. And the size of the echelle will be 400 mm × 500 mm, the reserved aluminum film is a small area.

4. Conclusions

The characteristics of the echelle, which has high diffraction orders and low zero-order efficiency, a new mirror–echelle structure is designed, and a method for mosaicking echelles is proposed that allows the "zero order" and the diffraction order to be detected simultaneously to remove the mosaicking errors. As the different types of the mosaicking errors, the adjustment devices are installed on the echelles respectively. As the summarized steps, the mosaicking experiment is carried out with two echelles of the PV values 0.452λ and 0.494λ. We get a mosaicked echelle, the PV is 0.592λ, the three-dimensional map of the wavefront shows that the surfaces of the two echelles are on the same plane and that the Strehl ratio can reach 0.947.

Acknowledgments

The authors acknowledge supports from National Natural Science Foundation of China (NSFC) (61605204, 61505204); Jilin Province Outstanding Youth Project in China (20170520167JH, 20180520190JH); Chinese Ministry of National Science and Technology Program (2016YFF0102006, 2016YFF0103304); National Basic Research Program of China (2014CB049500).

We thank David MacDonald, MSc, from Liwen Bianji, Edanz Editing China (www.liwenbianji.cn/ac), for editing the English text of a draft of this manuscript.

References

[1] N. Bonod, J. Neauport, Diffraction gratings: from principles to applications in high-intensity lasers, Adv. Opt. Photon. 8 (1) (2016) 156–199.
[2] T. Blasiak, S. Zheleznyak, History and construction of large mosaic diffraction gratings, Proc. SPIE. 4485 (2002) 370–377.
[3] S. Vogt, D. Schroeder, Introduction to the session on high resolution spectrographs, in: Instrumentation for Ground-Based Optical Astronomy©, Robinson, L.B., Springer-Verlag NewYork Inc, 1988.
[4] S. Mahadevan, L. Ramsey, J. Wright, M. Endl, S. Redman, C. Bender, A. Roy, S. Zonak, N. Troupe, L. Engel, S. Sigurdsson, A. Wolszczan, B. Zhao, The habitable zone planet finder: a proposed high-resolution NIR spectrograph for the Hobby Eberly Telescope to discover low-mass, Proc. SPIE. 77356 (2010) 77356X.
[5] G. Marchi, M. Plate, S. Birkmann, T. Böker, P. Ferruit, G. Giardino, P. Jakobsen, M. Sirianni J. Savignol, X. Gnata, R. Barho, M. Kosse, P. Mosner, B. Dorner, G. Cresci, F. Rosales-Ortega, M. Stuhlinger, T. Gross, Calibrating the position of images and spectra in the NIRSpec instrument for the James Webb Space Telescope, Proc. SPIE. 81500 (2011) 81500C.
[6] J. Pazder, S. Roberts, R. Abraham, A. Anthony, M. Fletcher, T. Hardy, D. Loop, S. Sun, WFOS: a wide field optical spectrograph for the Thirty Meter Telescope, Proc. SPIE. 62691 (2006) 62691X.
[7] J. Qiao, A. Kalb, T. Nguyen, J. Bunkenburg, D. Canning, J. Kelly, Demonstration of large-aperture tiled-grating compressors for highenergy, petawatt-class, chirped-pulse amplification systems, Opt. Lett. 33 (15) (2008) 1684–1686.
[8] J. Qiao, A. Kalb, M. Guardalben, G. King, D. Canning, J. Kelly, Large-aperture grating tiling by interferometry for petawatt chirped-pulse–amplification systems, Opt. Express 15 (15) (2007) 9562–9574.
[9] T. Kessler, J. Bunkenburg, H. Huang, A. Kozlov, D. Meyerhofer, Demonstration of coherent addition of multiple gratings for high-energy chirped-pulse-amplified lasers, Opt. Lett. 29 (6) (2004) 635–637.
[10] A. Cotel, C. Crotti, P. Audebert, C. Bris, C. Blanc, Tiled-grating compression of multiterawatt laser pulses, Opt. Lett. 32 (12) (2007) 1749–1751.
[11] A. Cotel, M. Castaing, P. Pichon, C. Blanc, Phased-array grating compression for high-energy chirped pulse amplification lasers, Opt. Express 15 (5) (2007) 2742–2752.
[12] Y. Ezaki, M. Tabata, M. Kihara, Y.Horiuchi, M.Endo, T.Jitsuno, Development of a segmented grating mount system for FIREX-1, J. Phys. Conf. Ser. 112 (2008) 032027.
[13] Y. Hu, L. Zeng, Grating mosaic based on image processing of far-field diffraction intensity patterns in two wavelengths, Appl. Opt. 46 (28) (2007) 7018–7025.
[14] Y. Hu, L. Zeng, L. Li, Method to mosaic gratings that relies on analysis of far-field intensity patterns in two wavelengths, Opt. Commun. 269 (2007) 285–290.
[15] L. Zeng, L. Li, Method of making mosaic gratings by using a two-color heterodyne interferometer containing a reference grating, Opt. Lett. 31 (2) (2006) 152–154.
[16] T. Harimoto, Far-field pattern analysis for an array grating compressor, Jpn. J. Appl. Phys. 43 (4A) (2004) 1362–1365.
[17] L. Shi, L. Zeng, L. Li, Fabrication of optical mosaic gratings with phase and attitude adjustments employing latent fringes and a red-wavelength dual-beam interferometer, Opt. Express 17 (24) (2009) 21530–21543.
[18] L. Shi, L. Zeng, Fabrication of optical mosaic gratings: a self-referencing alignment method, Opt. Express 19 (10) (2011) 8985–8993.
[19] Y. Lu, X. Qi, X. Li, H. Yu, S. Jiang, Bayanheshig, L. Yin, Removal of all mosaic grating errors in a single-interferometer system by a phase-difference reference window, Appl. Opt. 55 (28) (2016) 7997–8002.
[20] H. Zhou, L. Zeng, Optical mosaic method for orthogonally crossed gratings by utilizing information about both main periodic directions simultaneousl, Opt. Commun. 385 (2017) 181–187.
[21] Z. Li, S. Li, C. Wang, Y. Xu, F. Wu, Y. Li, Y. Leng, Stable and near Fourier-transform-limit 30fs pulse compression with a tiled grating compressor scheme, Opt. Express 23 (26) (2015) 33386–33395.
[22] H. Yu, X. Li, J. Zhu, H. Yu, X. Qi, S. Feng, Reducing the line curvature error of mechanically ruled gratings by interferometric control, Appl. Phys. B 117 (2014) 279–286.
[23] M. Cong, X. Qi, X. Mi, H. Yu, X. Li snd Y. Lu, Influence of incident light angles on mosaic grating errors in optical path for grating replication and mosaic, Opt. Precis. Eng. 25 (12) (2017) 3027–3033.